

Improving sample diversity of a pre-trained, class-conditional GAN by changing its class embeddings

Qi Li
 Auburn University
 qz10019@auburn.edu

Long Mai
 Adobe Inc.
 malong@adobe.com

Anh Nguyen
 Auburn University
 anh.ng8@gmail.com

Abstract

Mode collapse is a well-known issue with Generative Adversarial Networks (GANs) and is a byproduct of the unstable GAN training. We propose to improve the sample diversity of a pre-trained class-conditional generator by modifying its class embeddings in the direction of maximizing the log probability outputs of a classifier pre-trained on the same dataset. We improved the sample diversity of state-of-the-art ImageNet BigGANs at both 128×128 and 256×256 resolutions. By replacing the embeddings, we can also synthesize plausible images for Places365 using a BigGAN pre-trained on ImageNet.

1 INTRODUCTION

Generative Adversarial Networks (GANs) (Goodfellow et al., 2014) have achieved great success in generating high-fidelity images (Karras et al., 2018). However, they have a known problem of *mode collapse* i.e. the generated distribution does not capture all modes of the true distribution (Arjovsky and Bottou, 2017). Therefore, synthesizing images to match the 1000-class ImageNet dataset (Deng et al., 2009) has been a grand challenge to GANs whose samples were often far less diverse than the real data.

The recent class-conditional BigGAN (Brock et al., 2019) has reached an unprecedented state-of-the-art image quality and diversity on ImageNet by using large networks and batch sizes. However, interestingly, we observed that BigGAN samples from a set of ~ 50 classes exhibit substantially lower diversity than samples from other classes. For example, generated images

for `daisy` mostly show white flowers on green grass, but the training data includes images of daisies with a variety of colors and backgrounds (Fig. 1). Furthermore, samples for `window screen` not only have low diversity but also poor realism (see Fig. S5 for more low-diversity BigGAN samples). This phenomenon is intriguing given that BigGAN synthesizes photo-realistic images for many classes (Brock et al., 2019) i.e. the generator is *already capable* of painting a wide variety of images.

Why do we observe this stark contrast in BigGAN sample diversity for `window screen` or `daisy` vs. the other classes? Due to the notorious GAN training instability (Arjovsky and Bottou, 2017), BigGAN authors trained the generator until its performance collapsed and took the previous best snapshot as the final model. Therefore, the inferior sample diversity for a class y_c (e.g. `window screen`) may be because as BigGAN training collapsed, the generator’s parameters were corrupted in a way that degraded the capability of synthesizing the visual features needed for class y_c .

As it remains a myth how the synthesis capability degraded, improving the sample diversity for a mode-collapse class is non-trivial. First, re-training BigGANs requires expensive computation—the original 256×256 model took 48 hours of training on 256 Google Cloud TPUs. On more modest hardware of 8 \times V100 GPUs (Brock, 2019), the training is estimated to take 3–5 weeks and has not been found to match the results in Brock et al. (2019). Second, re-training or finetuning is likely to still cause a set of classes to collapse as we observed in the BigGAN-deep model released by Brock et al. (2019) (data not shown).

Surprisingly, we found that, for many classes, mode collapse can be substantially ameliorated (Fig. 1) by only modifying the class embeddings (i.e. keeping the generator unchanged). We improved the diversity by iteratively searching for an embedding input to a pre-trained BigGAN generator that yields random samples that maximize the probability scores by a pre-trained

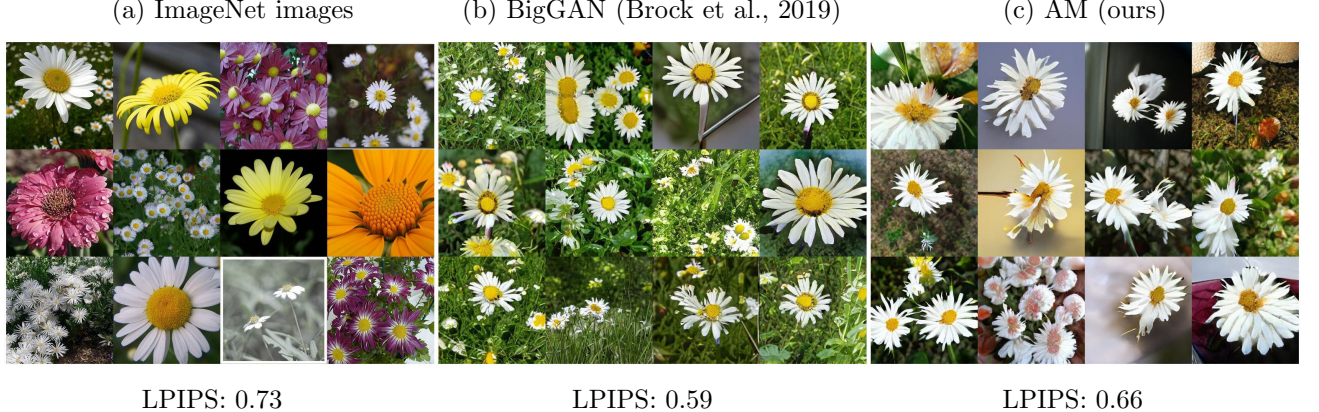


Figure 1: 256×256 BigGAN samples for some classes, here, *daisy* (b) are far less diverse than the real data (a). By updating *only* the class embeddings of BigGAN, our AM method (c) substantially improved the diversity, here reducing the LPIPS diversity gap by 50%. This result interestingly shows that the BigGAN generator itself was already capable of synthesizing such diverse images but the original embeddings limited the diversity.

image classifier (Fig. 2). Our main findings are:¹

1. The BigGAN class embeddings qualitatively capture class semantics (Sec. 3.1). For example, bird classes are nearby in t-SNE visualizations (Fig. S13).
2. Changing only the embeddings via our method was sufficient to match the diversity (via MS-SSIM and LPIPS metrics) of the real data while keeping the BigGAN generator frozen (Sec. 3.3). A human study found that our method produced more diverse (and similarly realistic) images compared to BigGAN (Sec. 3.5).
3. Our approach improved the sample diversity for two BigGANs released by the authors at both 256×256 and 128×128 resolutions (Sec. 3.7) and some mode-collapse BigGAN snapshots (Sec. 3.8).
4. By updating only the embedding matrix, we can harness a BigGAN pre-trained on ImageNet to generate images matching the Places365 scene categories (Sec. 3.9).

2 METHODS

2.1 Problem formulation

Activation maximization Let P be a pre-trained ImageNet classifier (Krizhevsky et al., 2012) that maps an image $\mathbf{x} \in \mathbb{R}^{256 \times 256 \times 3}$ onto a softmax probability distribution over 1,000 output classes.

Let G be a class-conditional generator, here a BigGAN pre-trained by Brock et al. (2019), that takes a class

¹All code and data will be available on github.com

embedding $\mathbf{c} \in \mathbb{R}^{128}$ and a latent vector $\mathbf{z} \in \mathbb{R}^{140}$ as inputs and outputs an image $G(\mathbf{c}, \mathbf{z}) \in \mathbb{R}^{256 \times 256 \times 3}$. The embedding matrix was learned during GAN training.

Intuitively, we search for an input class embedding \mathbf{c} of the generator G such that the output image $G(\mathbf{c}, \mathbf{z})$ for any random $\mathbf{z} \sim \mathcal{N}(0, I)$ would cause the classifier P to output a high probability for a target class \mathbf{y} (Fig. 2). Formally, we maximize the following objective given a pre-defined class y_c :

$$\max_{\mathbf{c}} L_{\text{AM}}(\mathbf{c}) = \mathbb{E}_{\mathbf{z} \sim \mathcal{N}(0, I)} \log P(\mathbf{y} = y_c \mid G(\mathbf{c}, \mathbf{z})) \quad (1)$$

We try to solve the above Activation Maximization (AM) problem (Nguyen et al., 2016) via mini-batch gradient descent. That is, we iteratively backpropagate through both the classifier P and the generator G and change the embedding \mathbf{c} to maximize the expectation of the log probabilities over a set \mathcal{Z} of random latent vectors.

Diversity regularization To explicitly encourage diversity, we add a regularization term that encourages a small change in the latent variable to yield a large change in the output image as in Yang et al. (2019):

$$\max_{\mathbf{c}} L_{\text{D}}(\mathbf{c}) = \mathbb{E}_{\mathbf{z}^i, \mathbf{z}^j \sim \mathcal{N}(0, I)} \frac{\|\phi(G(\mathbf{c}, \mathbf{z}^i)) - \phi(G(\mathbf{c}, \mathbf{z}^j))\|}{\|\mathbf{z}^i - \mathbf{z}^j\|} \quad (2)$$

where $\phi(\cdot)$ is a feature extractor. In Yang et al. (2019), $\phi(\cdot)$ is an identity function to encourage pixel-wise diversity. We also tested with $\phi(\cdot)$ being outputs of the conv5 layer and the output softmax layer of AlexNet.

In practice, we maximized the objective via 10 unique

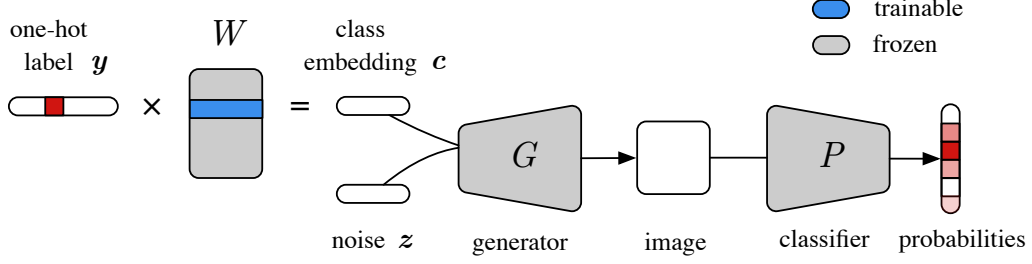


Figure 2: To improve the samples for a target class represented by a one-hot vector y , we iteratively take steps to find an embedding c (i.e. a row in the embedding matrix W) such that all the generated images $\{G(c, z^i)\}$, for different random noise vectors $z^i \sim \mathcal{N}(0, I)$, would be (1) classified as the target class y ; and (2) diverse i.e. yielding different softmax probability distributions. We backpropagate through both the frozen, pre-trained generator G and classifier P and perform gradient descent over batches of random latent vectors $\{z^i\}$.

pairs of (z^i, z^j) selected from \mathcal{Z} . In sum, we encouraged the samples to be in a target class y and diverse via the full objective function below:

$$\max_c L_{\text{AM-D}}(c) = L_{\text{AM}} + \lambda L_{\text{D}} \quad (3)$$

where λ is a hyperparameter to be tuned.

2.2 Datasets

While the generators and classifiers were pre-trained on the full 1000-class ImageNet 2012 dataset, we evaluated our methods on a subset of 50 classes (hereafter, ImageNet-50) where we qualitatively found BigGAN samples exhibit the lowest diversity. The selection of 50 classes were informed by two diversity metrics (see below) but decided by humans before the study.

2.3 Evaluation metrics

Because there is currently no single metric that is able to capture the multi-dimensional characteristics of an image set (Borji, 2019), we chose a broad range of common metrics to measure the sample diversity and realism separately.

Diversity We measured the intra-class diversity by randomly sampling 200 image pairs from an image set and computing the MS-SSIM (Odena et al., 2017) and LPIPS (Zhang et al., 2018) scores for each pair. For each method, we computed a mean score across the 50 classes \times 200 image pairs.

Realism To measure the sample realism, we used the Inception Score (IS) with 10 splits (Salimans et al., 2016), the Fréchet Inception Distance (FID) (Heusel et al., 2017), and the Inception Accuracy (IA) (Odena et al., 2017). These three metrics were computed for every set of 50,000 images = 50 classes \times 1000 images.

2.4 Networks

Classifiers Our default image classifier is AlexNet (Krizhevsky et al., 2012) pre-trained on the 1000-class ImageNet 2012 dataset. Note that other ImageNet classifiers can also be used as shown in Sec. 3.3.

Generators We used two pre-trained ImageNet BigGAN generators (Brock et al., 2019), a 256×256 and a 128×128 model, released by the authors in PyTorch. For the purpose of studying diversity, all generated images in this paper were sampled from the full, non-truncated prior distribution (Brock et al., 2019).

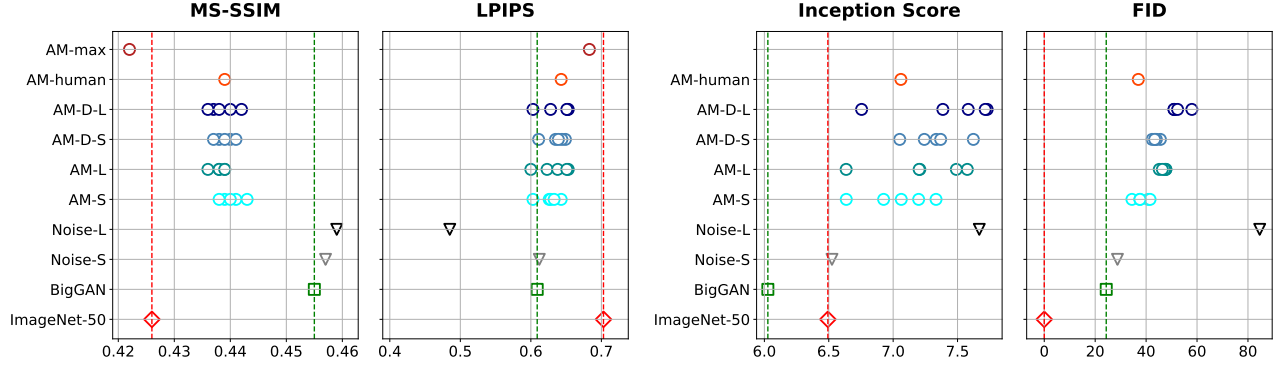
3 EXPERIMENTS AND RESULTS

3.1 Semantically meaningful BigGAN class embeddings

We observed via t-SNE visualizations (Maaten and Hinton, 2008) that the class embeddings learned by BigGAN captured well the semantics of the ImageNet classes. That is, we projected 1000 class embeddings $c^i \in \mathbb{R}^{128}$ onto a 2-D t-SNE space. Interestingly, the embeddings for the low-diversity ImageNet-50 classes are far from being random i.e. they were reasonably located in the neighborhood of related concepts (Fig. S13; the *daisy* embedding is near other flowers and plants). The semantically meaningful t-SNE arrangements of the BigGAN class embeddings motivated us to search in the neighborhood of an original embedding to find a new vector that yields more diverse images (see the following sections).

3.2 Adding noise to or finetuning the class embeddings did not improve diversity

Adding noise A naive attempt to improve the diversity is adding small random noise to the embedding vector of a low-diversity class. Across 50 classes,



(a) Diversity comparison in MS-SSIM and LPIPS metrics.

(b) Realism comparison in IS and FID metrics.

Figure 3: Each point in the four plots is a mean score across 50 classes from one AM optimization trial or one BigGAN model. The ultimate goal here is to close the gap between the BigGAN samples (---) and the ImageNet-50 distribution (----) in all four metrics. Naively adding noise degraded the embeddings in both diversity (MS-SSIM and LPIPS) and quality (IS and FID) scores i.e. the black and gray ∇ actually moved away from the red lines. Our optimization trials, on average, closed the *diversity* gap by $\sim 50\%$ i.e. the AM circles are half way in between the green and red dash lines (a). However, there was a trade-off between diversity vs. quality i.e. on the IS and FID metrics, the AM circles went further away from the red line (b).

we found that adding small noise $\sim \mathcal{N}(0, 0.1)$ almost did not quantitatively change the image quality and diversity (Fig. 3; Noise-S) while adding larger noise $\sim \mathcal{N}(0, 0.3)$ degraded the samples on both criteria (Fig. 3; Noise-L). For example, daisy samples gradually turned into human-unrecognizable rubbish images as we increased the noise (Fig. S4).

Finetuning Another strategy to improve sample diversity is to finetune BigGANs. However, how to finetune a BigGAN to improve its sample diversity is an open question. The BigGAN pre-trained model would start to degrade if we kept training it using the original hyperparameters as reported in Brock et al. (2019).

To minimize the GAN training instability and compare with other approaches in this paper, we only finetuned one embedding at a time, keeping the other embeddings and all parameters in the generator and discriminator frozen. Because Brock et al. (2019) only released the discriminator for their 128×128 generator but not for the 256×256 model, we only finetuned the 128×128 model. For each class, we added a small amount of noise $\sim \mathcal{N}(0, 0.1)$ to the associated embedding vector and finetuned it using the original BigGAN training objective for 10 iterations until the training collapsed. Across 50 classes \times 5 trials, quantitatively, finetuning did not improve the sample diversity but lowered the realism (Fig. 4; purple Δ vs. green \square).

3.3 Activation Maximization was effective in improving 256×256 sample diversity

The previous results showed that modifying the embeddings following random directions (i.e. adding noise) or the more informed gradients from BigGAN discriminators (i.e. finetuning) failed to improve sample diversity. Here, we propose to update an embedding following the gradients from an image classifier to maximize its log probabilities (Fig. 2).

We found two strategies to be effective: (1) searching within a small region around the original embeddings (AM-S); (2) searching within a large region around the mean embedding (AM-L).

Hyperparameters For AM-S, we randomly initialized the embedding within a Gaussian ball of radius 0.1 around the original embedding. We used a learning rate of 0.01. For AM-L, we randomly initialized the embedding around the mean of all 1000 embeddings and used a larger learning rate of 0.1. For both settings, we maximized Eq. 1 using the Adam optimizer and its default hyperparameters for 200 steps. We re-sampled a set $\mathcal{Z} = \{\mathbf{z}^i\}_{20}$ every 20 steps. Every step, we kept the embeddings within $[-0.59, 0.61]$ by clipping. To evaluate each trial, we used the embedding from the last step and sampled 1000 images per class. We ran 5 trials per class with different random initializations.

Classifiers In the preliminary experiments, we tested four ImageNet classifiers: AlexNet, Inception-v3 (Szegedy et al., 2016), ResNet-50 (He et al., 2016), and a ResNet-50 (Engstrom et al., 2019) that is robust

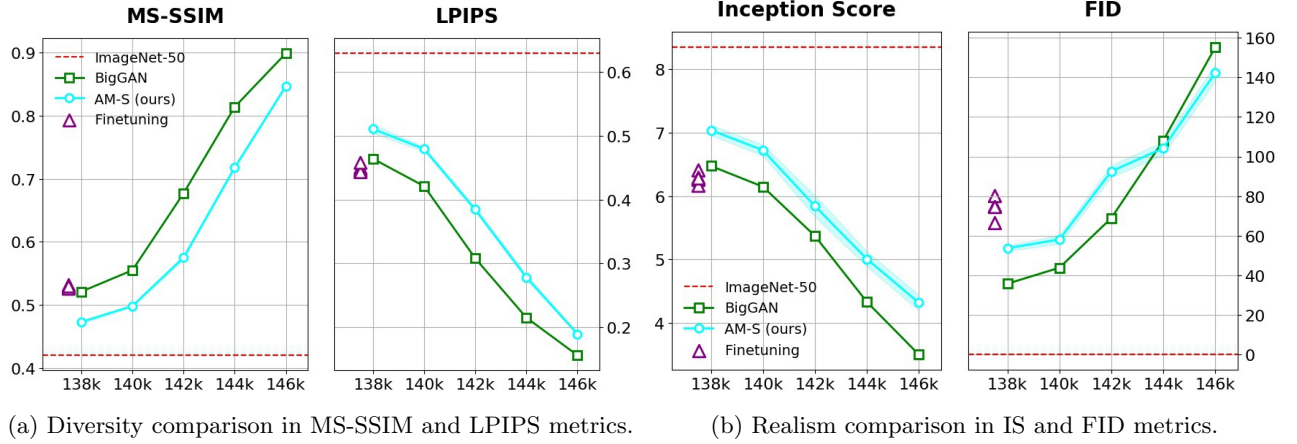


Figure 4: Each point in the four plots is a mean score across 50 classes and five AM-S trials or one 128×128 BigGAN model. Finetuning the 138k snapshot neither improved the sample diversity nor realism (purple Δ vs. green \square). Optimizing the embeddings via AM-S consistently improved the diversity in both MS-SSIM and LPIPS (a). IS and FID metrics disagree on whether AM-S (cyan \circ) sample quality is better or worse than that of the BigGAN samples. See Fig. 6 for a side-by-side comparison of the samples from these five snapshots.

to pixel-wise noise. By default, we resized the BigGAN output images to the appropriate input resolution of each classifier. With Inception-v3, we achieved an FID score that is (a) substantially better than those for the other three classifiers (Table S2; 30.24 vs. 48.74), and (b) similar to that of the original BigGAN (30.24 vs. 31.36). The same trends were observed with the Inception Accuracy metrics (Table S2). However, we did not find any substantial qualitative differences among the samples of the four treatments. Therefore, we chose AlexNet because of its fastest run time.

Results Across 50 classes \times 5 trials, we found that both AM-S and AM-L produced samples of higher diversity than the original BigGAN samples. For both MS-SSIM and LPIPS, on average, our AM methods reduced the gap between the original BigGAN and the real data by $\sim 50\%$ (Fig. 3a; AM-S and AM-L vs. BigGAN). For all 50 classes, we always found at least 1 out of 10 trials (i.e. both methods combined) that yielded samples that match the real data in MS-SSIM or LPIPS scores (Fig. 3a; AM-max vs. ImageNet-50). The statistics also align with our qualitative observations that AM samples often contain a more diverse set of object poses, shapes and backgrounds than the BigGAN samples (see Figs. S9–S11).

In terms of IA and FID scores, AM samples have lower realism than BigGAN samples (Table S1). Given the known inflation issues with IS scores (Barratt and Sharma, 2018), here, our IS scores (Fig. 3b) suggest that AM did not improve the sample realism upon BigGAN. However, for some classes e.g. window screen, AM was able to turn the original rubbish images into a diverse set of recognizable samples (Fig. S10c).

3.4 Explicitly encouraging diversity yielded worse sample realism

Inspired by Yang et al. (2019), here, we try to improve the sample diversity further by incorporating a diversity regularizer into the previous two AM-S and AM-L methods (Sec. 2.1) to produce two new variants AM-D-S and AM-D-L. We tested encouraging diversity in the (1) image space; (2) conv5 feature space; and (3) softmax outputs of AlexNet and found they can qualitatively bias the optimization towards different interesting spaces of diversity.

However, the addition of the regularizer quantitatively improved the diversity but at a large cost of lower sample quality (Fig. 3b AM-S vs. AM-D-S and AM-L vs. AM-D-L). Similarly, the IA scores of the AM-D methods were consistently lower than those of the original AM methods (Table S1). See Sec. S1 for more details.

3.5 Humans rated AM samples more diverse and similarly realistic

While quantitative image evaluation metrics are imperfect, we ran a human study to compare the AM vs. original BigGAN samples. For each class, across all 20 embeddings from 5 trials \times 4 methods (AM-S, AM-L, AM-D-S, and AM-D-L), we manually chose one embedding that qualitatively is a balance between diversity and realism to sample images to represent our AM method in the study. As a reference, this set of AM images were more diverse and less realistic than BigGAN samples according to the quantitative metrics (Fig. 3; AM-human vs. BigGAN).

Experiments We created two separate online surveys for diversity and realism, respectively. For each class, the diversity survey showed a panel of 8×8 AM images side-by-side a panel of 8×8 BigGAN samples and asked participants to rate which panel is more diverse on the scale of 1–5. That is, 1 or 5 denotes the left or right panel is clearly more diverse, while 3 indicates both sets are similarly diverse. For each class, the AM and BigGAN panels were randomly positioned left or right. The realism survey was a duplicate of the diversity except that each panel only showed 3×3 images so that participants could focus more on the details.

Results For both tests, we had 52 participants who are mostly university students and do not work with Machine Learning or GANs. On average, AM samples were rated to be more diverse and similarly realistic compared to BigGAN samples. That is, AM images were given better than the neutral score of 3, i.e. 2.24 ± 0.85 in diversity and 2.94 ± 1.15 in realism. Also, AM samples were rated to be more diverse in 42/50 classes and more realistic in 22/50 classes. See Figs. S9–S11 for your own comparisons.

3.6 AM embeddings still capture semantics and enable realistic interpolations

While the new embeddings discovered by our AM methods changed the generated samples entirely for many classes e.g. `window screen`, we observed that interpolating in the latent or embedding spaces still yields realistic intermediate samples (Fig. 5). See Figs. S17–S19 for more examples of interpolation between \mathbf{z} pairs and between \mathbf{c} pairs i.e. classes.



Figure 5: Interpolation between a \mathbf{z} pair in the `window screen` class using the original BigGAN embedding (top) yields similar and unrealistic samples. The same interpolation with the embedding found by AM (bottom) produced realistic intermediate samples.

In addition, the 50 embeddings found by AM when projected onto a 2-D t-SNE space still capture the class semantics similarly to the original BigGAN embeddings (see Fig. S16 for side-by-side comparisons).

3.7 Generalization to a 128×128 BigGAN

To test whether our method generalizes to a different GAN at a lower resolution, we applied our AM-S

method (see Sec. 3.3) to a pre-trained 128×128 BigGAN released by Brock (2019). As in previous experiments, we ran 50 classes \times 5 trials in total. To evaluate each trial, we used the last-step embedding to sample 1000 images per class.

Consistent with the result on the 256×256 resolution, here, AM-S improved the diversity over the pre-trained model on both MS-SSIM and LPIPS (Fig. 4a; 138k). In terms of quality, FID and IS showed a mixed result of whether AM-S sample realism is lower or higher. See Fig. S12 for random side-by-side image comparisons.

3.8 Generalization to different training snapshots of 128×128 BigGAN

We have shown that BigGAN sample diversity can be improved substantially by changing only the embeddings (Sec. 3.3) which revealed that the generator was actually capable of synthesizing those diverse images. Here, we test how much sample diversity and quality can be improved by AM as the BigGAN training gradually collapses, which might corrupt not only the embeddings but also the generator’s parameters.

Experiments We took the pre-trained 128×128 BigGAN model (saved at the 138k-th iteration) and continued training it for 9000 more iterations with the same hyperparameters as in Brock (2019). We applied the AM-S method with the same hyperparameters as in Sec. 3.7 to four BigGAN snapshots captured at the 140k, 142, 144k, and 146k iteration, respectively.

Results AM-S consistently improved the sample diversity of all snapshots. For some classes, AM qualitatively improved both the sample diversity and quality (Figs. 6 and S6–S8). However, the sample diversity and realism of both AM-S and the original BigGAN gradually dropped together (Fig. 4; AM-S vs. BigGAN). The result suggests that, as the GAN training gradually collapsed, the generator might have been so corrupted that changing the class embeddings alone is not sufficient to significantly improve the samples.

3.9 BigGAN trained on ImageNet can synthesize scene images for Places365

Our study has revealed that the BigGAN generator pre-trained on ImageNet is able to synthesize a wide variety of images. Here, we test whether it is possible to re-use the same ImageNet generator to synthesize images for a different target dataset of Places365 (Zhou et al., 2017), which contains 365 classes of scene images. For evaluation, we randomly chose 50 out of 365 classes in Places365 (hereafter, Places-50).

Mean initialization We ran the AM-L algorithm for 5 trials per class with the same hyperparameters as

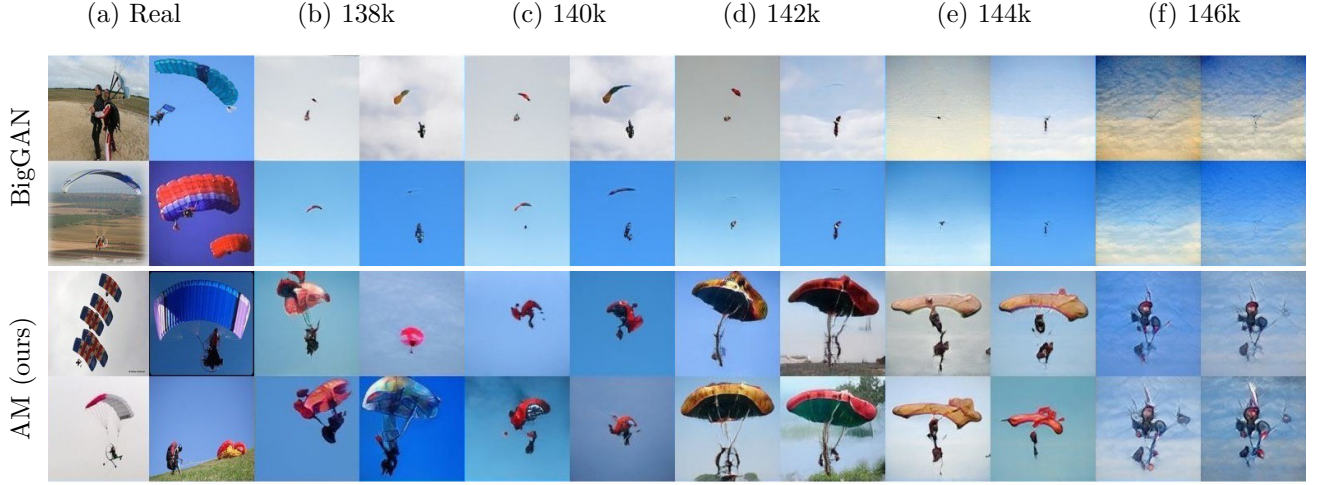


Figure 6: For the **parachute** class, the original 128×128 BigGAN samples (top panel) mostly contained tiny parachutes in the sky (b) and gradually degraded into blue sky images only (c–f). AM (bottom panel) instead exhibited a more diverse set of close-up and far-away parachutes (b) and managed to paint the parachutes for nearly-collapsed models (e–f). The samples in this figure correspond to the five snapshots (138k—146k) reported in the quantitative comparison in Fig. 4. See Figs. S6, S7, S8 for more qualitative comparisons.

in Sec. 3.3 but with a ResNet-18 classifier (He et al., 2016) pre-trained on Places365.

Top-5 initialization Besides initializing from the mean embeddings, we also tested initializing from the top-5 embeddings whose 10 random generated samples were given the highest average accuracy scores by the Places365 classifier. For example, to synthesize the **hotel room** images for Places365, the top-1 embedding in the ImageNet dataset is for class **quilt** (Fig. 7). We reproduced 5 AM-L trials but each was initialized with a unique embedding among the top-5.

Baseline We used the original BigGAN samples for the top-1 ImageNet classes found from the top-5 initialization procedure above as a baseline.

Results AM-L found many class embeddings that produced plausible images for Places365 scene classes using the same ImageNet BigGAN generator. For example, to match the **hotel room** class which does not exist in ImageNet, AM-L synthesized bedroom scenes with lights and windows whereas the top-1 class (**quilt**) samples mostly shows beds with blankets (Fig. 7). See Figs. S20, S21, S22, S23 for more image comparisons.

Compared to the baseline, AM-L samples have substantially higher realism in FID (41.25 vs. 53.15) and in ResNet-18 Accuracy scores (0.49 vs. 0.17). In terms of diversity, AM-L and the baseline performed similarly and both were slightly worse than the real images in MS-SSIM (0.42 vs. 0.43) and LPIPS (0.65 vs. 0.70). See Table S3 for more detailed quantitative results.

4 RELATED WORK

Latent space traversal Searching in the latent space of a GAN generator network to synthesize images has been shown effective for many tasks including (1) in-painting (Yeh et al., 2017); (2) image editing (Zhu et al., 2016); (3) creating natural adversarial examples (Zhao et al., 2018); or (4) feature visualization (Nguyen et al., 2019). While all prior work in this line of research optimized the latent variable \mathbf{z} , we instead optimize the class embeddings \mathbf{c} of a class-conditional generator over a set of random \mathbf{z} vectors.

Our approach might be the most related to Plug & Play Generative Networks (PPGN) (Nguyen et al., 2017) in that both methods sample from the joint distribution $p_G(\mathbf{x}, \mathbf{y})$ defined by a generator and a pre-trained classifier. While Nguyen et al. (2017) trained an unconditional generator that inverts the features of an ImageNet classifier, our method is generally applicable to any pre-trained class-conditional generator. Importantly, our goal is novel—to improve the sample diversity of any pre-trained class-conditional generator (here, BigGANs) by changing its class embeddings.

Improving sample quality Two methods, MHGAN (Turner et al., 2019) and DRS (Azadi et al., 2019), have recently been proposed to improve the samples of a pre-trained GAN by harnessing the discriminator to reject low-probability generated samples. However, these methods are able to only improve sample *quality*, but not diversity. In addition, they assume that the discriminator is (a) available, which may not



Figure 7: AM-L generated plausible images for two Places365 classes, hotel room (top) and plaza (bottom), which do not exist in the ImageNet training set of the generator. For example, AM-L synthesizes images of squares with buildings and people in the background for the plaza class (c) while the samples from the top-1 ImageNet class, here, parking meter, shows parking meters on the street (b). Similarly, AM-L samples for the hotel room class has the unique touches of lighting, lamps, and windows (c) that do not exist in the BigGAN samples for the quilt class (b). See Figs. S20, S21, S22, and S23 for more side-by-side image comparisons.

always be the case e.g. in the official BigGAN releases (Brock et al., 2019); and (b) optimally trained for their samplers to recover exactly the true distribution. Similar to MH-GAN and PPGN, our method is similar to a Markov chain Monte Carlo (MCMC) sampler that has no rejection steps. A major difference is that we only perform the iterative optimization *once* to update the embedding matrix. After a desired embedding is found, our subsequent samplings of images are fast following standard GANs. In contrast, MH-GAN, DRS, and PPGN samplers often require many rejection or update steps to sample a single image.

Improving sample diversity Many GAN regularization tricks have been introduced to encourage the samples to be diverse (see Wang et al. (2019) for a survey). However, all prior methods require re-training GANs from scratch, which can be computationally expensive e.g. in the BigGAN’s case. Fine-tuning GANs may be a more efficient approach (Wang et al., 2018). However, finetuning (1) requires both the pre-trained generator and discriminator, which is not always available in practice, and (2) is subject to the known train-

ing instability issues (as in Sec. 3.2). Here, our method is not subject to the above issues and can be viewed as finetuning only the embedding layer but using an AM objective instead of a GAN objective.

Generalization Understanding the image synthesis capability of a trained GAN generator is an active research area. Recent findings showed that GANs trained on a dataset of scene images contain neurons that can paint common objects such as “trees” or “doors” (Bau et al., 2019). Jahanian et al. (2019) found that BigGAN is able to perform some general image transforms such as zoom, rotate or brightness adjustment up to a certain limit. However, these methods optimize only the latent variable (Jahanian et al., 2019) or both the latent and the generator parameters (Bau et al., 2019), but not the embeddings as ours.

5 CONCLUSION

We showed that the low sample diversity of pre-trained GAN generators can be improved by simply changing the class embeddings, not the generator. Note that

one could “recover” the missing modes using our AM methods and improve the sample quality further by sampling from a truncated prior distribution (Brock et al., 2019). Compared to finetuning or re-training BigGANs from scratch, our method is more tractable even considering that one has to run five 200-step optimization trials to find a desired class embedding.

Acknowledgements

We thank Chirag Agarwal, Naman Bansal, and Michael Alcorn for valuable discussions and helpful feedback on the drafts. Especially, we thank Michael Alcorn for a code example. AN is supported by the National Science Foundation under Grant No. 1850117, Amazon Research Credits, Auburn University, Adobe Inc, and donations from Nvidia.

References

Arjovsky, M. and Bottou, L. (2017). Towards principled methods for training generative adversarial networks. In *5th International Conference on Learning Representations, ICLR 2017, Toulon, France, April 24-26, 2017, Conference Track Proceedings*.

Azadi, S., Olsson, C., Darrell, T., Goodfellow, I., and Odena, A. (2019). Discriminator rejection sampling. In *International Conference on Learning Representations*.

Barratt, S. and Sharma, R. (2018). A note on the inception score. *arXiv preprint arXiv:1801.01973*.

Bau, D., Zhu, J.-Y., Strobelt, H., Zhou, B., Tenenbaum, J. B., Freeman, W. T., and Torralba, A. (2019). Visualizing and understanding generative adversarial networks. In *International Conference on Learning Representations*.

Borji, A. (2019). Pros and cons of gan evaluation measures. *Computer Vision and Image Understanding*, 179:41–65.

Brock, A. (2019). ajbrock/biggan-pytorch: The author’s officially unofficial pytorch biggan implementation. <https://github.com/ajbrock/BigGAN-PyTorch>. (Accessed on 07/25/2019).

Brock, A., Donahue, J., and Simonyan, K. (2019). Large scale GAN training for high fidelity natural image synthesis. In *International Conference on Learning Representations*.

Deng, J., Dong, W., Socher, R., Li, L.-J., Li, K., and Fei-Fei, L. (2009). Imagenet: A large-scale hierarchical image database. In *Computer Vision and Pattern Recognition, 2009. CVPR 2009. IEEE Conference on*, pages 248–255. IEEE.

Engstrom, L., Ilyas, A., Santurkar, S., Tsipras, D., Tran, B., and Madry, A. (2019). Learning perceptually-aligned representations via adversarial robustness. *arXiv preprint arXiv:1906.00945*.

Goodfellow, I., Pouget-Abadie, J., Mirza, M., Xu, B., Warde-Farley, D., Ozair, S., Courville, A., and Bengio, Y. (2014). Generative adversarial nets. In *NIPS*.

He, K., Zhang, X., Ren, S., and Sun, J. (2016). Deep residual learning for image recognition. In *Proceedings of the IEEE conference on computer vision and pattern recognition*, pages 770–778.

Heusel, M., Ramsauer, H., Unterthiner, T., Nessler, B., and Hochreiter, S. (2017). Gans trained by a two time-scale update rule converge to a local nash equilibrium. In *Advances in Neural Information Processing Systems*, pages 6626–6637.

Jahanian, A., Chai, L., and Isola, P. (2019). On the “steerability” of generative adversarial networks. *arXiv preprint arXiv:1907.07171*.

Karras, T., Aila, T., Laine, S., and Lehtinen, J. (2018). Progressive growing of GANs for improved quality, stability, and variation. In *International Conference on Learning Representations*.

Krizhevsky, A., Sutskever, I., and Hinton, G. E. (2012). Imagenet classification with deep convolutional neural networks. In *Advances in neural information processing systems*, pages 1097–1105.

Maaten, L. v. d. and Hinton, G. (2008). Visualizing data using t-sne. *Journal of machine learning research*, 9(Nov):2579–2605.

Nguyen, A., Clune, J., Bengio, Y., Dosovitskiy, A., and Yosinski, J. (2017). Plug & play generative networks: Conditional iterative generation of images in latent space. In *Proceedings of the IEEE Conference on Computer Vision and Pattern Recognition*, pages 4467–4477.

Nguyen, A., Dosovitskiy, A., Yosinski, J., Brox, T., and Clune, J. (2016). Synthesizing the preferred inputs for neurons in neural networks via deep generator networks. In *Advances in Neural Information Processing Systems*, pages 3387–3395.

Nguyen, A., Yosinski, J., and Clune, J. (2019). Understanding neural networks via feature visualization: A survey. *arXiv preprint arXiv:1904.08939*.

Odena, A., Olah, C., and Shlens, J. (2017). Conditional image synthesis with auxiliary classifier gans. In *Proceedings of the 34th International Conference on Machine Learning-Volume 70*, pages 2642–2651. JMLR. org.

Salimans, T., Goodfellow, I., Zaremba, W., Cheung, V., Radford, A., and Chen, X. (2016). Improved techniques for training gans. In *Advances in neural information processing systems*, pages 2234–2242.

Szegedy, C., Vanhoucke, V., Ioffe, S., Shlens, J., and Wojna, Z. (2016). Rethinking the inception architecture for computer vision. In *Proceedings of the IEEE conference on computer vision and pattern recognition*, pages 2818–2826.

Turner, R., Hung, J., Frank, E., Saatchi, Y., and Yosinski, J. (2019). Metropolis-Hastings generative adversarial networks. In Chaudhuri, K. and Salakhutdinov, R., editors, *Proceedings of the 36th International Conference on Machine Learning*, volume 97 of *Proceedings of Machine Learning Research*, pages 6345–6353, Long Beach, California, USA. PMLR.

Wang, Y., Wu, C., Herranz, L., van de Weijer, J., Gonzalez-Garcia, A., and Raducanu, B. (2018). Transferring gans: generating images from limited data. In *Proceedings of the European Conference on Computer Vision (ECCV)*, pages 218–234.

Wang, Z., She, Q., and Ward, T. E. (2019). Generative adversarial networks: A survey and taxonomy. *arXiv preprint arXiv:1906.01529*.

Yang, D., Hong, S., Jang, Y., Zhao, T., and Lee, H. (2019). Diversity-sensitive conditional generative adversarial networks. In *International Conference on Learning Representations*.

Yeh, R. A., Chen, C., Yian Lim, T., Schwing, A. G., Hasegawa-Johnson, M., and Do, M. N. (2017). Semantic image inpainting with deep generative models. In *Proceedings of the IEEE Conference on Computer Vision and Pattern Recognition*, pages 5485–5493.

Zhang, R., Isola, P., Efros, A. A., Shechtman, E., and Wang, O. (2018). The unreasonable effectiveness of deep features as a perceptual metric. In *Proceedings of the IEEE Conference on Computer Vision and Pattern Recognition*, pages 586–595.

Zhao, Z., Dua, D., and Singh, S. (2018). Generating natural adversarial examples. In *International Conference on Learning Representations*.

Zhou, B., Lapedriza, A., Khosla, A., Oliva, A., and Torralba, A. (2017). Places: A 10 million image database for scene recognition. *IEEE transactions on pattern analysis and machine intelligence*, 40(6):1452–1464.

Zhu, J.-Y., Krähenbühl, P., Shechtman, E., and Efros, A. A. (2016). Generative visual manipulation on the natural image manifold. In *European Conference on Computer Vision*, pages 597–613. Springer.

SUPPLEMENTARY MATERIAL

Method	IS (10 splits) (higher=better)	FID (lower=better)	Inception Accuracy (higher=better)	MS-SSIM (lower=better)	LPIPS (higher=better)
1. ImageNet-50 (real)	6.49 ± 0.63	N/A	0.90	0.43 ± 0.04	0.70 ± 0.08
2. BigGAN	6.03 ± 0.87	24.34	0.87	0.46 ± 0.05	0.61 ± 0.09
3. Noise-S	6.53 ± 0.86	28.75	0.82	0.46 ± 0.05	0.61 ± 0.09
4. Noise-L	7.67 ± 0.95	84.61	0.36	0.46 ± 0.05	0.49 ± 0.04
5. AM-S					
a. Best LPIPS trial	7.33 ± 0.73	40.82	0.72	0.44 ± 0.05	0.64 ± 0.08
b. Average	7.03 ± 0.71	38.39	0.74	0.44 ± 0.05	0.63 ± 0.08
6. AM-L					
a. Best LPIPS trial	7.49 ± 0.81	47.25	0.64	0.44 ± 0.04	0.65 ± 0.08
b. Average	7.22 ± 0.79	46.86	0.68	0.44 ± 0.05	0.63 ± 0.08
7. AM-D-S					
a. Best LPIPS trial	7.62 ± 0.90	45.61	0.66	0.44 ± 0.04	0.65 ± 0.08
b. Average	7.32 ± 0.80	43.78	0.68	0.44 ± 0.05	0.64 ± 0.08
8. AM-D-L					
a. Best LPIPS trial	7.58 ± 0.84	50.94	0.64	0.44 ± 0.04	0.65 ± 0.08
b. Average	7.43 ± 0.85	52.68	0.61	0.44 ± 0.05	0.64 ± 0.08

Table S1: We compared Activation Maximization (AM) samples with the BigGAN samples and the real ImageNet-50 images on two diversity metrics (MS-SSIM and LPIPS) and three realism metrics, Inception Score (IS), Fréchet Inception Distance (FID), and Inception Accuracy (IA). ImageNet-50 is a subset of ImageNet that contains 50 classes where BigGAN samples exhibit limited diversity (see Sec. 2.2). For each AM method, we ran 50 classes \times 5 trials and reported here (a) the trial with the best LPIPS score and (b) the average across 5 runs. In MS-SSIM and LPIPS, all AM trials consistently produced more diverse samples than the BigGAN samples. However, FID and IA scores indicated that AM samples are worse in realism compared to the original BigGAN samples. See Fig. 3 for some graphical plots of this table.

S1 Explicitly encouraging diversity yielded worse sample realism

We found that in $\sim 2\%$ of the AM-S and AM-L trials, the optimization converged at a class embedding that yields similar images for different random latent vectors. Here, we try to improve the sample diversity further by incorporating a specific regularization term into the AM formulation (as described in Sec. 2.1).

Experiments In the preliminary experiments, we tested encouraging diversity in the (1) image space; (2) `conv5` feature space; and (3) softmax outputs of AlexNet. We observed that the pixel-wise regularizer can improve the diversity of background colors (Fig. S1) and tends to increase the image contrast upon a high λ multiplier (Fig. S1c). In contrast, the impact of the `conv5` diversity regularizer is less noticeable (Fig. S2). Encouraging diversity in the softmax output distribution can yield novel scenes e.g. growing more flowers in `monarch butterfly` images (Fig. S3c).

While each level of diversity has its own benefits for specific applications, here, we chose to perform more tests with the softmax diversity to encourage samples to be more diverse *semantically*. That is, we re-ran the AM-S and AM-L experiments with an additional softmax diversity term (Eq. 3) and a coefficient $\lambda = 2$ (see Fig. S3). We call these two AM methods with the diversity term AM-D-S and AM-D-L.

Results We found that the addition of the regularizer did not improve the diversity substantially but lowered the sample quality (Fig. 3b AM-S vs. AM-D-S and AM-L vs. AM-D-L). Similarly, the IA scores of the AM-D methods were consistently lower than those of the original AM methods (Table S1).

Method	IS (10 splits) (higher=better)	FID (lower=better)	Inception Accuracy (higher=better)	MS-SSIM (lower=better)	LPIPS (higher=better)
1. ImageNet-30 (Real)	4.18 \pm 0.61	n/a	0.92	0.42 \pm 0.04	0.70 \pm 0.08
2. BigGAN	3.71 \pm 0.74	31.36	0.91	0.45 \pm 0.05	0.61 \pm 0.09
3. AM-L Random					
a. AlexNet	5.06 \pm 0.97	46.85	0.71	0.43 \pm 0.04	0.66 \pm 0.08
b. Inception-v3	4.29 \pm 0.56	31.62	0.87	0.44 \pm 0.04	0.65 \pm 0.08
c. ResNet-50	5.36 \pm 0.75	47.23	0.70	0.44 \pm 0.04	0.68 \pm 0.09
d. Robust ResNet-50	4.59 \pm 0.69	43.65	0.76	0.43 \pm 0.05	0.63 \pm 0.08
4. AM-D-S					
a. AlexNet	5.31 \pm 0.60	48.74	0.69	0.43 \pm 0.04	0.66 \pm 0.08
b. Inception-v3	4.23 \pm 0.51	30.24	0.88	0.44 \pm 0.04	0.65 \pm 0.08
c. ResNet-50	5.78 \pm 1.00	52.01	0.66	0.43 \pm 0.04	0.68 \pm 0.08
d. Robust ResNet-50	4.51 \pm 0.79	41.74	0.78	0.44 \pm 0.04	0.63 \pm 0.09

Table S2: A comparison of four different classifiers (a–d) across two preliminary AM settings across 30 random classes from the ImageNet-50 low-diversity dataset (see Sec. 2.2). The ImageNet-30 statistics here were computed from 30,000 images = 30 classes \times 1000 images. Similarly, for BigGAN (Row 2) and AM-L and AM-D-S methods (Row 3–4), we generated 1000 256 \times 256 samples per class. We computed the statistics for each initialization method from 5 trials, each with a different random seed. With AM-L (Sec. 3.3), we maximized the log probabilities and used a large learning rate of 0.1. With AM-D-S (Sec. 3.4), we maximized both the log probabilities and a softmax diversity regularization term, and used a small learning rate of 0.01. In sum, across both settings, AM consistently obtained the highest FID and Inception Accuracy (IA) scores with the Inception-v3 classifier (b). That is, it is possible to maximize the FID and IA scores when using Inception-v3 as the classifier in the AM formulation. However, qualitatively, we did not find the AM samples with Inception-v3 to be substantially different from the others.

Method	IS (10 splits) (higher=better)	FID (lower=better)	ResNet-18 Accuracy (higher=better)	MS-SSIM (lower=better)	LPIPS (higher=better)
1. Places-50 (real)	12.17 \pm 1.01	N/A	0.57	0.42 \pm 0.04	0.70 \pm 0.06
2. BigGAN	8.19 \pm 0.9	53.15	0.17	0.42 \pm 0.05	0.66 \pm 0.07
3. AM-L with Mean Initialization					
Trial 1	8.32 \pm 0.89	42.38	0.51	0.43 \pm 0.05	0.64 \pm 0.07
Trial 2	8.39 \pm 0.83	44.11	0.48	0.43 \pm 0.05	0.64 \pm 0.07
Trial 3	8.45 \pm 0.84	42.98	0.46	0.43 \pm 0.05	0.65 \pm 0.07
Trial 4	7.03 \pm 0.71	38.39	0.49	0.43 \pm 0.05	0.64 \pm 0.07
Trial 5	7.03 \pm 0.71	38.39	0.49	0.43 \pm 0.04	0.65 \pm 0.07
Average	7.03 \pm 0.51	41.25	0.49	0.43 \pm 0.05	0.65 \pm 0.07
4. AM-L with Top-5 Initialization					
Trial 1	8.60 \pm 0.88	46.92	0.47	0.43 \pm 0.05	0.65 \pm 0.07
Trial 2	8.45 \pm 0.81	41.09	0.52	0.43 \pm 0.05	0.65 \pm 0.07
Trial 3	8.13 \pm 0.71	40.35	0.48	0.43 \pm 0.05	0.65 \pm 0.07
Trial 4	8.20 \pm 0.79	43.56	0.47	0.43 \pm 0.05	0.65 \pm 0.07
Trial 5	8.37 \pm 0.75	39.49	0.50	0.43 \pm 0.05	0.65 \pm 0.07
Average	8.35 \pm 0.79	42.28	0.49	0.43 \pm 0.05	0.65 \pm 0.07

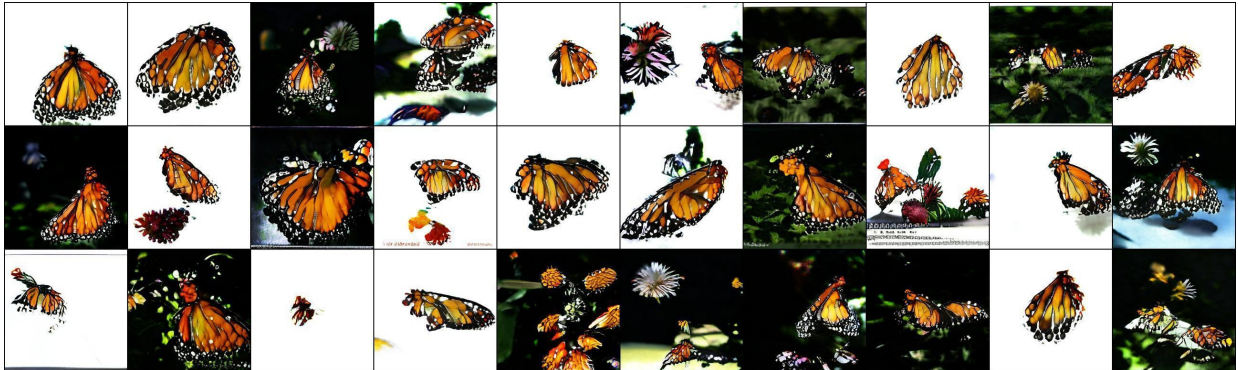
Table S3: A comparison of Places-50, BigGAN and AM images. We randomly chose 50 classes in Places365 (i.e. Places-50) to be the evaluation dataset for the experiments in Sec. 3.9. The Places-50 statistics here were computed from 50,000 images = 50 classes \times 1000 images that were randomly selected from the training set of Places365. For BigGAN (Sec. 3.9), we chose the class embedding whose 10 random samples yielded the highest accuracy score for each target Places-50 class and generated 1000 samples per class. With AM-L mean initialization and AM-L top-5 initialization (Sec. 3.9), we maximized the log probabilities and used a large learning rate of 0.1. We found that samples from AM (Row 3–4) are of similar diversity but better quality than BigGAN samples.



(a) AM alone without the diversity term (i.e. $\lambda = 0$ in Eq. 3).



(b) AM with the pixel-wise diversity term (i.e. $\lambda = 0.01$ in Eq. 3).



(c) AM with the pixel-wise diversity term (i.e. $\lambda = 0.1$ in Eq. 3).



(d) AM with the pixel-wise diversity term (i.e. $\lambda = 1.0$ in Eq. 3).

Figure S1: The monarch butterfly class (323) samples generated by Activation Maximization (AM) methods when increasing the multiplier λ of a pixel-wise diversity regularization term in Eq. 3.



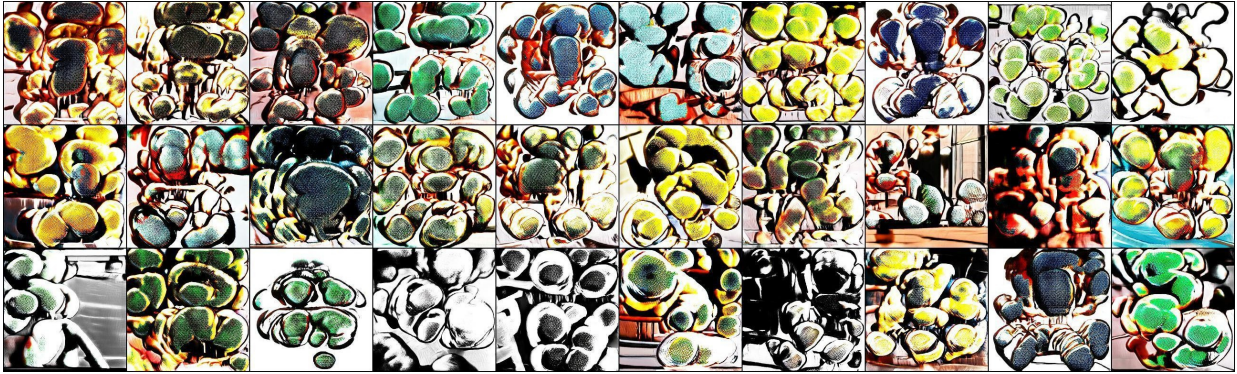
(a) AM alone without the diversity term (i.e. $\lambda = 0$ in Eq. 3).



(b) AM with a feature diversity term (i.e. $\lambda = 0.01$ in Eq. 3).



(c) AM with a feature diversity term (i.e. $\lambda = 0.1$ in Eq. 3).



(d) AM with a feature diversity term (i.e. $\lambda = 1.0$ in Eq. 3).

Figure S2: The monarch butterfly class (323) samples generated by Activation Maximization (AM) methods when increasing the multiplier λ of a conv5 feature diversity regularization term in Eq. 3.



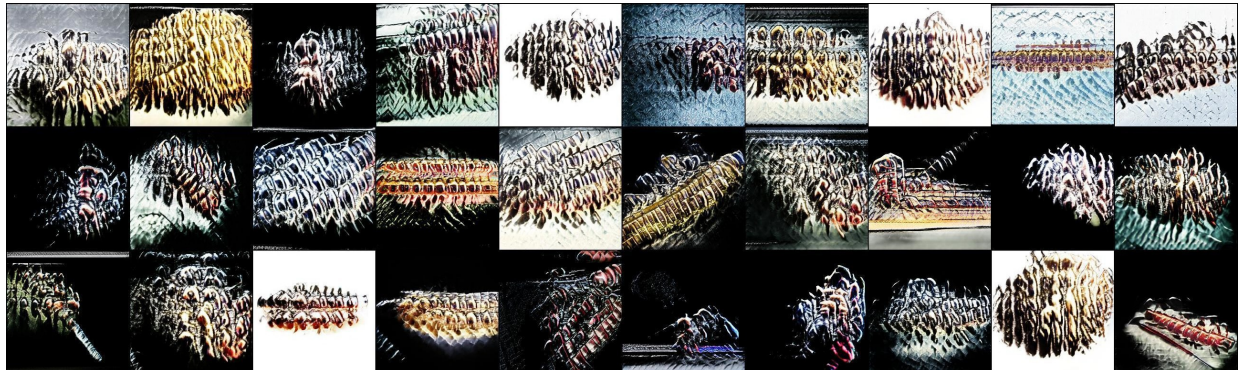
(a) AM alone without the diversity term (i.e. $\lambda = 0$ in Eq. 3).



(b) AM with a softmax diversity term (i.e. $\lambda = 2$ in Eq. 3).



(c) AM with a softmax diversity term (i.e. $\lambda = 10$ in Eq. 3).



(d) AM with a softmax diversity term (i.e. $\lambda = 100$ in Eq. 3).

Figure S3: The monarch butterfly class (323) samples generated by Activation Maximization (AM) methods when increasing the multiplier λ of a softmax probability diversity regularization term in Eq. 3.



(a) BigGAN samples generated with the original **daisy** class embedding (no noise).



(b) BigGAN samples generated with the **daisy** class embedding $\mathbf{c}' = \mathbf{c} + \epsilon$ where noise $\epsilon \sim \mathcal{N}(0, 0.1)$.



(c) BigGAN samples generated with the **daisy** class embedding $\mathbf{c}' = \mathbf{c} + \epsilon$ where noise $\epsilon \sim \mathcal{N}(0, 0.3)$.



(d) BigGAN samples generated with the **daisy** class embedding $\mathbf{c}' = \mathbf{c} + \epsilon$ where noise $\epsilon \sim \mathcal{N}(0, 0.5)$.

Figure S4: BigGAN samples when increasing the amount of noise added to the original **daisy** class embedding vector. That is, four panels (a-d) are generated using the same set of 30 latent vectors $\{\mathbf{z}^i\}_{30}$ but with a different class embedding \mathbf{c}' .

(a) ImageNet images



(b) BigGAN samples (Brock et al., 2019)

(a) Samples from the **window screen** class (904).



(b) Samples from the **manhole cover** class (640).



(c) Samples from the **greenhouse** class (580).



(d) Samples from the **cardoon** class (946).

Figure S5: Example mode-collapse classes from the ImageNet-50 subset where BigGAN samples (right) exhibit substantially lower diversity compared to the real data (left).



(a) ImageNet samples from the parachute class.



(b) BigGAN samples (left) and AM samples (right), both generated using the BigGAN 138k snapshot.



(c) BigGAN samples (left) and AM samples (right), both generated using the BigGAN 140k snapshot.



(d) BigGAN samples (left) and AM samples (right), both generated using the BigGAN 142k snapshot.



(e) BigGAN samples (left) and AM samples (right), both generated using the BigGAN 144k snapshot.



(f) BigGAN samples (left) and AM samples (right), both generated using the BigGAN 146k snapshot.

Figure S6: Applying our AM method to 5 different 128×128 BigGAN training snapshots (b-f) yielded samples (right) that qualitatively are more diverse and recognizable to be from the parachute class compared to the original BigGAN samples (left). While the original BigGAN samples are almost showing only the blue sky (d-f), AM samples show large and colorful parachutes.



(a) ImageNet samples from the pickelhaube class.



(b) BigGAN samples (left) and AM samples (right), both generated using the BigGAN 138k snapshot.



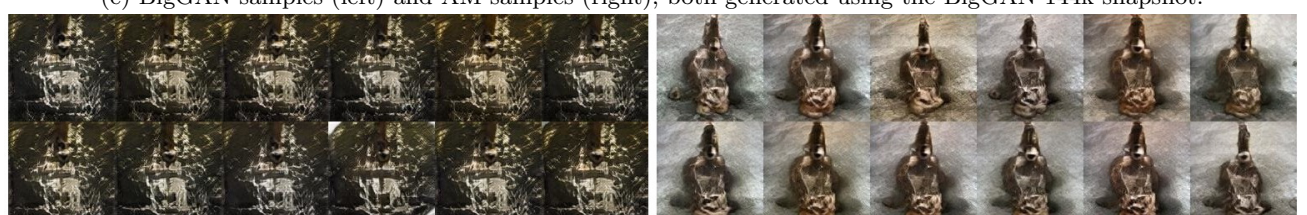
(c) BigGAN samples (left) and AM samples (right), both generated using the BigGAN 140k snapshot.



(d) BigGAN samples (left) and AM samples (right), both generated using the BigGAN 142k snapshot.



(e) BigGAN samples (left) and AM samples (right), both generated using the BigGAN 144k snapshot.



(f) BigGAN samples (left) and AM samples (right), both generated using the BigGAN 146k snapshot.

Figure S7: The same figure as Fig. S6 but for the pickelhaube class (715).



(a) ImageNet samples from the digital clock class.



(b) BigGAN samples (left) and AM samples (right), both generated using the BigGAN 138k snapshot.



(c) BigGAN samples (left) and AM samples (right), both generated using the BigGAN 140k snapshot.



(d) BigGAN samples (left) and AM samples (right), both generated using the BigGAN 142k snapshot.



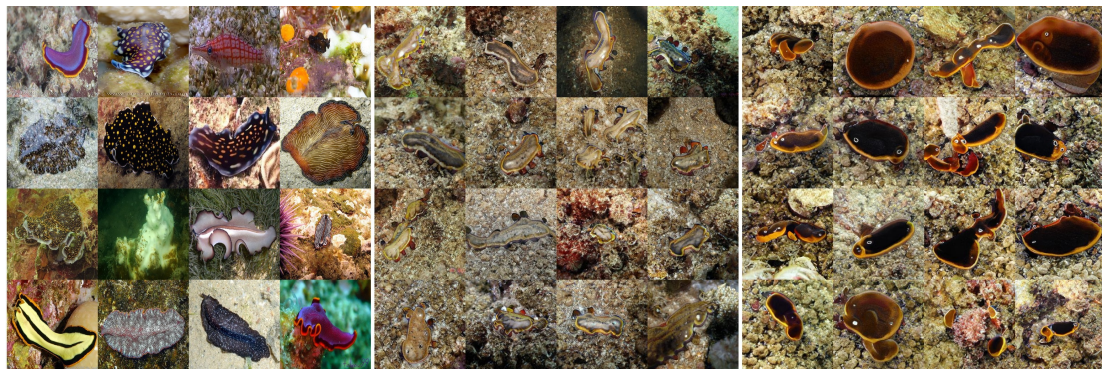
(e) BigGAN samples (left) and AM samples (right), both generated using the BigGAN 144k snapshot.



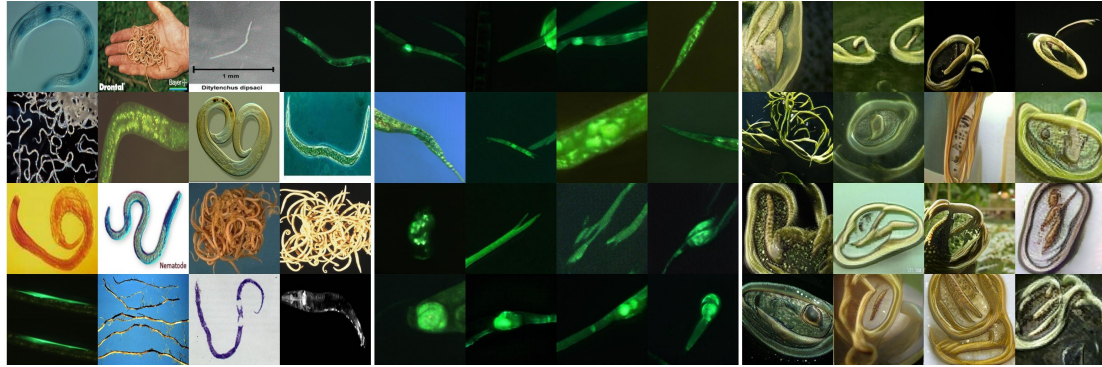
(f) BigGAN samples (left) and AM samples (right), both generated using the BigGAN 146k snapshot.

Figure S8: The same figure as Fig. S6 but for the digital clock class (530).

(a) ImageNet



(a) Samples from the flatworm class (110).



(b) Samples from the nematode class (111).

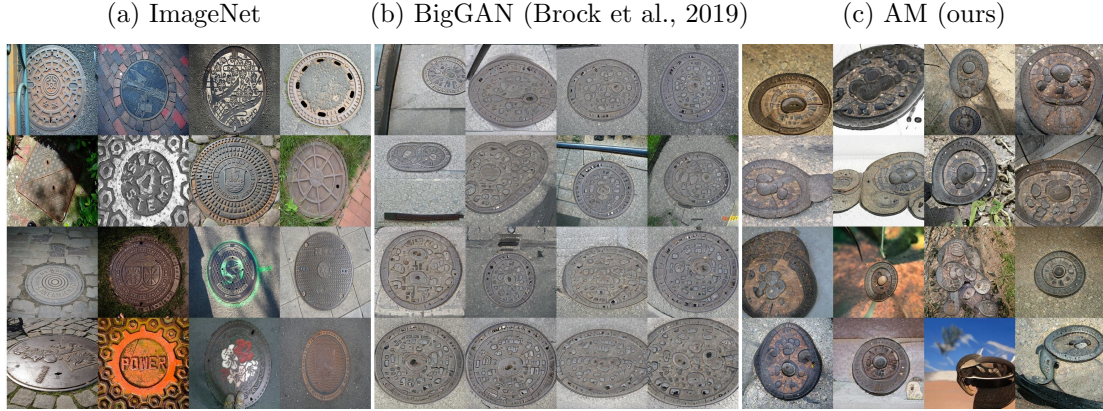


(c) Samples from the brass class (458).



(d) Samples from the greenhouse class (580).

Figure S9: A comparison between the 256×256 samples from the ImageNet training set (a), the original BigGAN model (b), and our AM method (c) for four ImageNet-50 low-diversity classes. AM samples (c) are of similar quality but higher diversity than the original BigGAN samples (b). See <https://drive.google.com/drive/folders/14qiLdaslnxfsCMnlBa4n1iE01EUUYUjQ?usp=sharing> for the high-resolution version of this figure.



(a) Samples from the manhole cover class (640).



(b) Samples from the spider web class (815).



(c) Samples from the window screen class (904).



(d) Samples from the cardoon class (946).

Figure S10: A comparison between the 256×256 samples from the ImageNet training set (a), the original BigGAN model (b), and our AM method (c) for four ImageNet-50 low-diversity classes. AM samples (c) are of similar quality but higher diversity than the original BigGAN samples (b). See <https://drive.google.com/drive/folders/14qiLdaslnxfsCMnlBa4n1iE01EUUYUjQ?usp=sharing> for the high-resolution version of this figure.

(a) ImageNet



(a) Samples from the **pineapple** class (953).



(b) Samples from the **custard apple** class (956).



(c) Samples from the **carbonara** class (959).



(d) Samples from the **pizza** class (963).

Figure S11: A comparison between the 256×256 samples from the ImageNet training set (a), the original BigGAN model (b), and our AM method (c) for four ImageNet-50 low-diversity classes. AM samples (c) are of similar quality but higher diversity than the original BigGAN samples (b). See <https://drive.google.com/drive/folders/14qiLdaslnxfsCMnlBa4n1iE01EUUYUjQ?usp=sharing> for the high-resolution version of this figure.

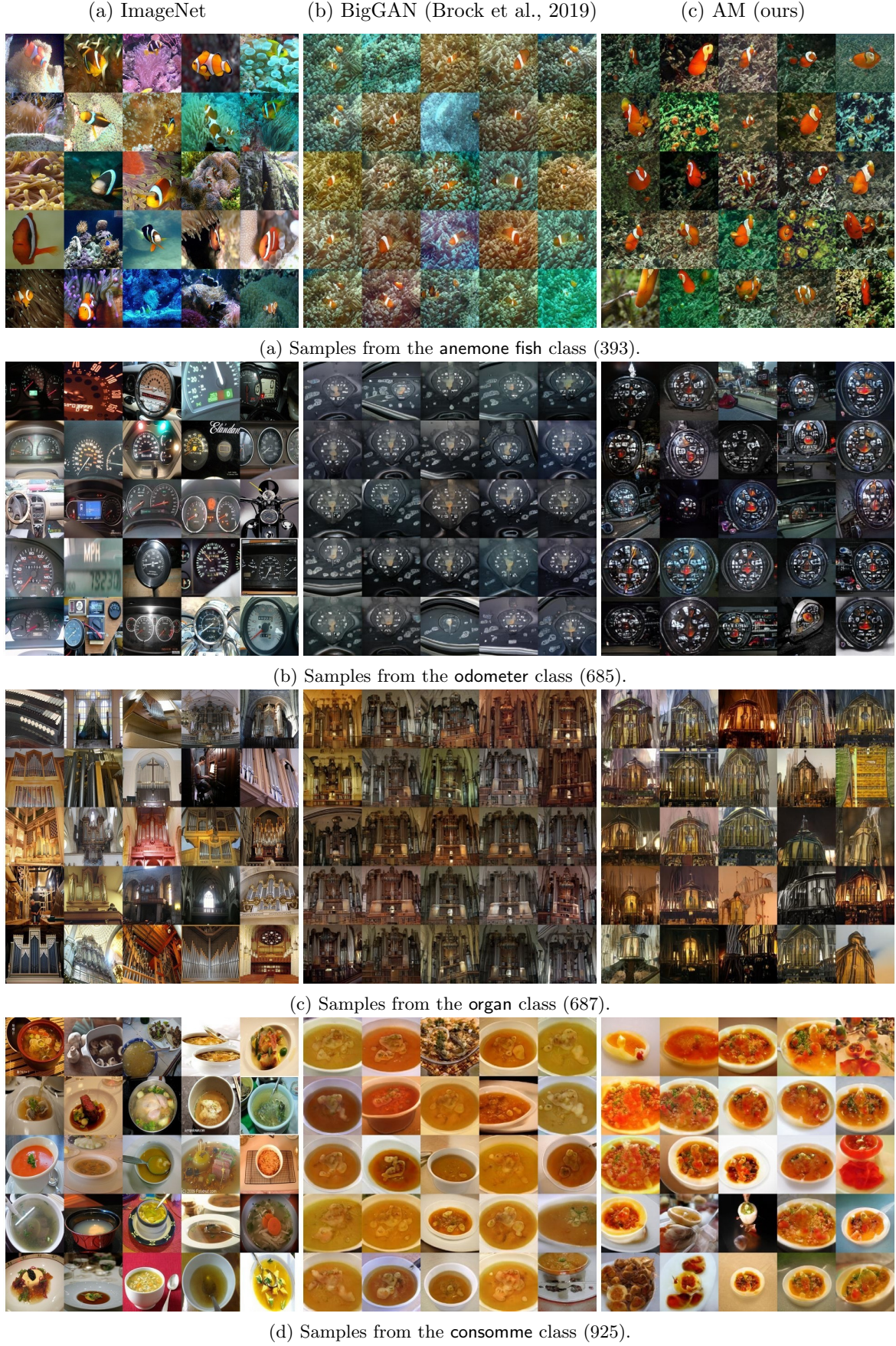
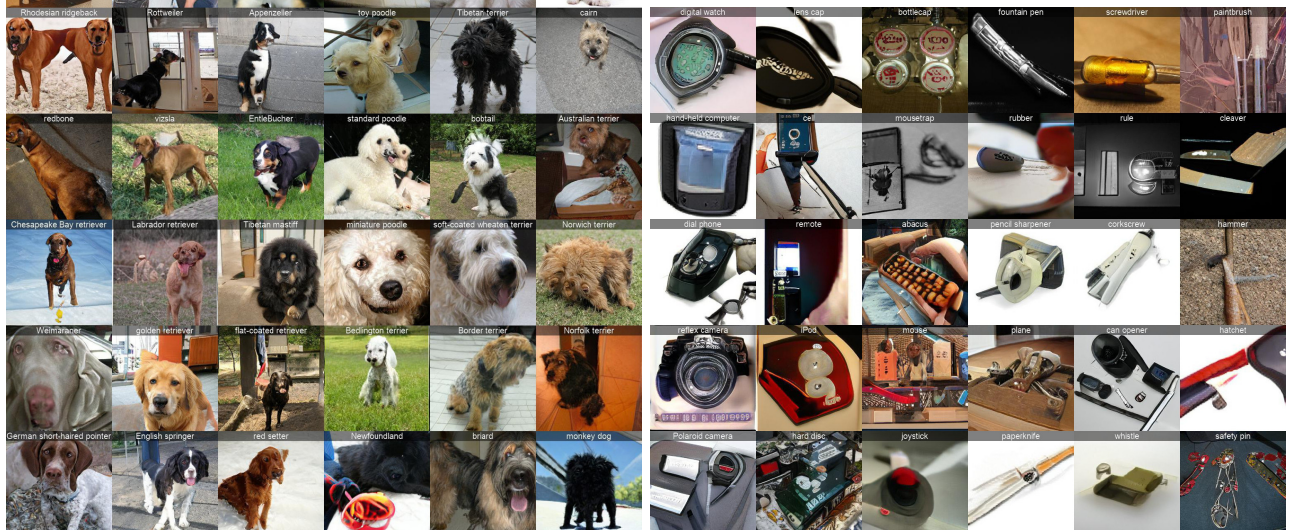


Figure S12: A comparison between the 128×128 samples from the ImageNet training set (a), the original BigGAN model (b), and our AM method (c) for four ImageNet-50 low-diversity classes. AM samples (c) are of similar quality but higher diversity than the original BigGAN samples (b).



(b) Most of birds are located nearby.



(a) Most dogs are located nearby.

(c) Man-made tools are located nearby.

Figure S13: Three zoom-in panels cropped out from the t-SNE visualization of 1000 original BigGAN class embeddings in Fig. S14. The BigGAN class embeddings are arranged semantically meaningful in the 2-D t-SNE visualization.



Figure S14: A 25×40 t-SNE 2-D visualization for 1000 original BigGAN class embeddings. At each t-SNE grid, we show a random BigGAN sample for the corresponding class. See <https://drive.google.com/open?id=1Jm1sUs1k45xmP71y2o4yYSNzhID8qadB> for the high-resolution version of this figure.



Figure S15: The same figure as Fig. S14 except that here we replace the 50 original BigGAN embeddings for the ImageNet-50 classes with the 50 embeddings found by AM (the highlighted cells). See https://drive.google.com/open?id=1i77bItzL_tM9S8nZ7E58EAUtTb1DFSL for a high-resolution version of this figure.



(a) Original BigGAN embeddings.

(b) Embeddings found by AM.

Figure S16: After modifying the 50 embeddings via AM, we re-plotted the t-SNE visualization for the entire 1000 classes. We color-code each class here with a unique border color. The arrangement of the original embeddings (left) are similar to that of the AM embeddings (right). For example, the *daisy* and *spider web* were nearby before (left) and also after AM modifications (right). In total, there are 21 classes that appear in both panels here. For each class, here, we show a random image i.e. the original BigGAN samples for the left panel and the samples generated by the AM embeddings. The left (a) and right panels (b) are crops from the Figs. S14 and S15, respectively.



(a) Interpolation in the embedding space between sea urchin (leftmost) and German shepherd (rightmost).



(b) Interpolation in the embedding space between honeycomb (leftmost) and junco bird (rightmost).



(c) Interpolation in the embedding space between hot pot (leftmost) and cheeseburger (rightmost).

Figure S17: The interpolation samples between c class-embedding pairs with latent vectors z held constant. In each panel, the top row shows the interpolation between two original 256×256 BigGAN embeddings while the bottom row shows the interpolation between an embedding found by AM (leftmost) and the original BigGAN embedding (right). In sum, the interpolation samples with the AM embeddings (bottom panels) appear to be similarly plausible as the original BigGAN interpolation samples (top panels).



(a) Interpolation in the embedding space between **window screen** (leftmost) and **water tower** (rightmost).



(b) Interpolation in the embedding space between **espresso** (leftmost) and **pop bottle** (rightmost).



(c) Interpolation in the embedding space between **agaric** (leftmost) and **bolete** (rightmost).

Figure S18: The interpolation samples between c class-embedding pairs (from related ImageNet classes e.g. agaric and bolete are both mushrooms) with latent vectors z held constant. In each panel, the top row shows the interpolation between two original 256×256 BigGAN embeddings while the bottom row shows the interpolation between an embedding found by AM (leftmost) and the original BigGAN embedding (right). In sum, the interpolation samples with the AM embeddings (bottom panels) appear to be similarly plausible as the original BigGAN interpolation samples (top panels).



(a) Interpolation in the latent space between two z vectors with the same **greenhouse** class embedding.



(b) Interpolation in the latent space between two z vectors with the same **window screen** class embedding.



(c) Interpolation in the latent space between two z vectors with the same **espresso** class embedding.



(d) Interpolation in the latent space between two z vectors with the same **daisy flower** class embedding.

Figure S19: The interpolation samples between z latent-vector pairs with the same class embeddings. The z -interpolation samples with the AM embeddings (bottom panels) appear to be similarly plausible as the original BigGAN interpolation samples (top panels). For the **window screen** class (b), AM recovered the human-unrecognizable BigGAN samples into a plausible interpolation between two scenes of windows.



Figure S20: A comparison between the 256×256 samples from the Places365 training set (a), the BigGAN samples generated for the ImageNet class whose 10 random samples were given the highest accuracy for the target class in Places365 (b), and our AM samples (c). AM samples (c) are of similar diversity but better quality than the original BigGAN samples (b). See https://drive.google.com/drive/folders/1L-1ULPf0f_5-98I7emYw860PDu3Fjxn?usp=sharing for a high-resolution version of this figure.

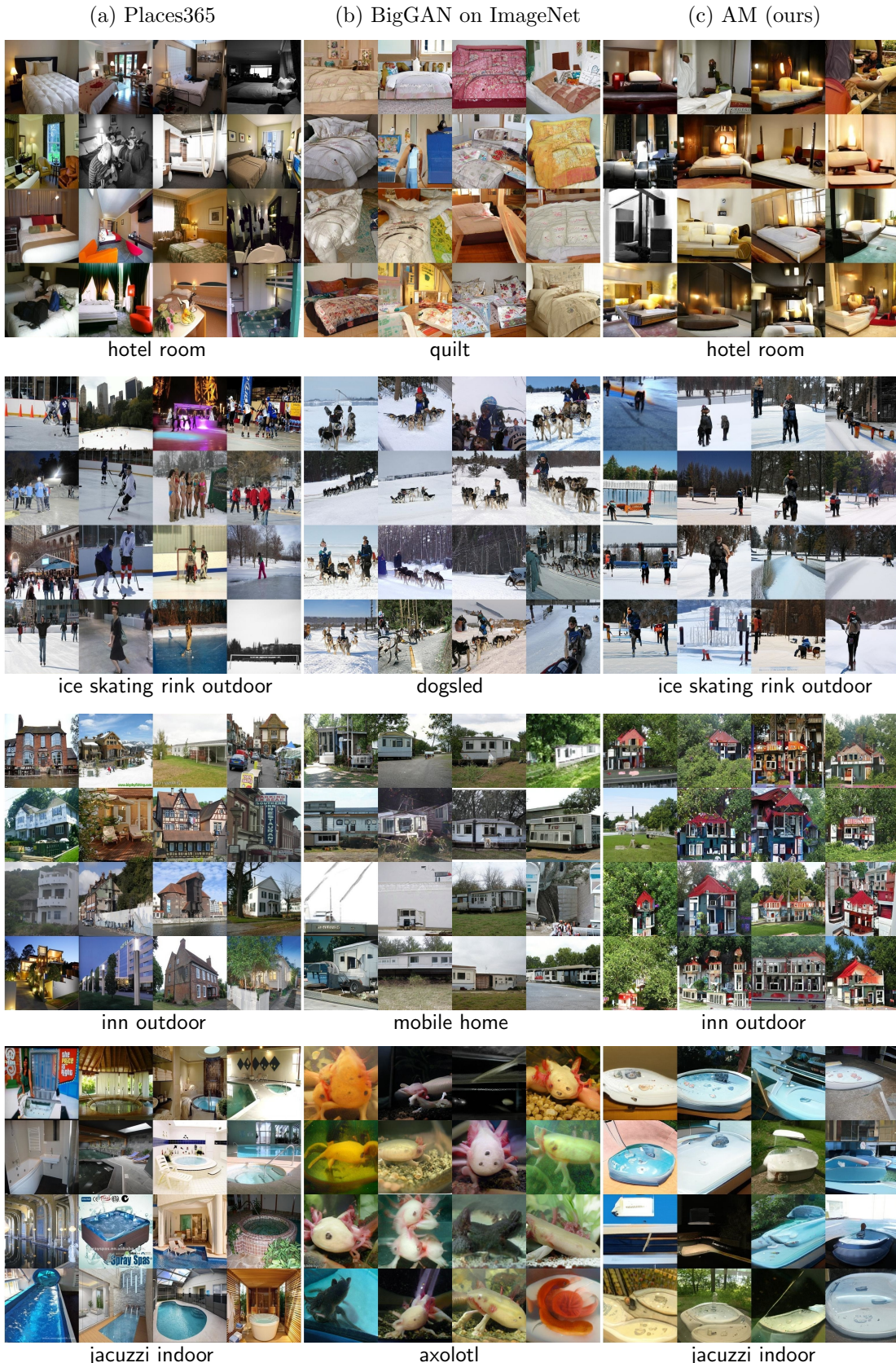


Figure S21: The same figure as Fig. S20 but for four different classes. While the ImageNet axolotl class samples were given the highest accuracy (bottom panel), they are qualitatively more different from the real jacuzzi images compared to the AM samples which shows the bathtubs. See https://drive.google.com/drive/folders/1L-1ULPf0f_5-98I7emYW860PDu3Fjxn?usp=sharing for a high-resolution version of this figure.

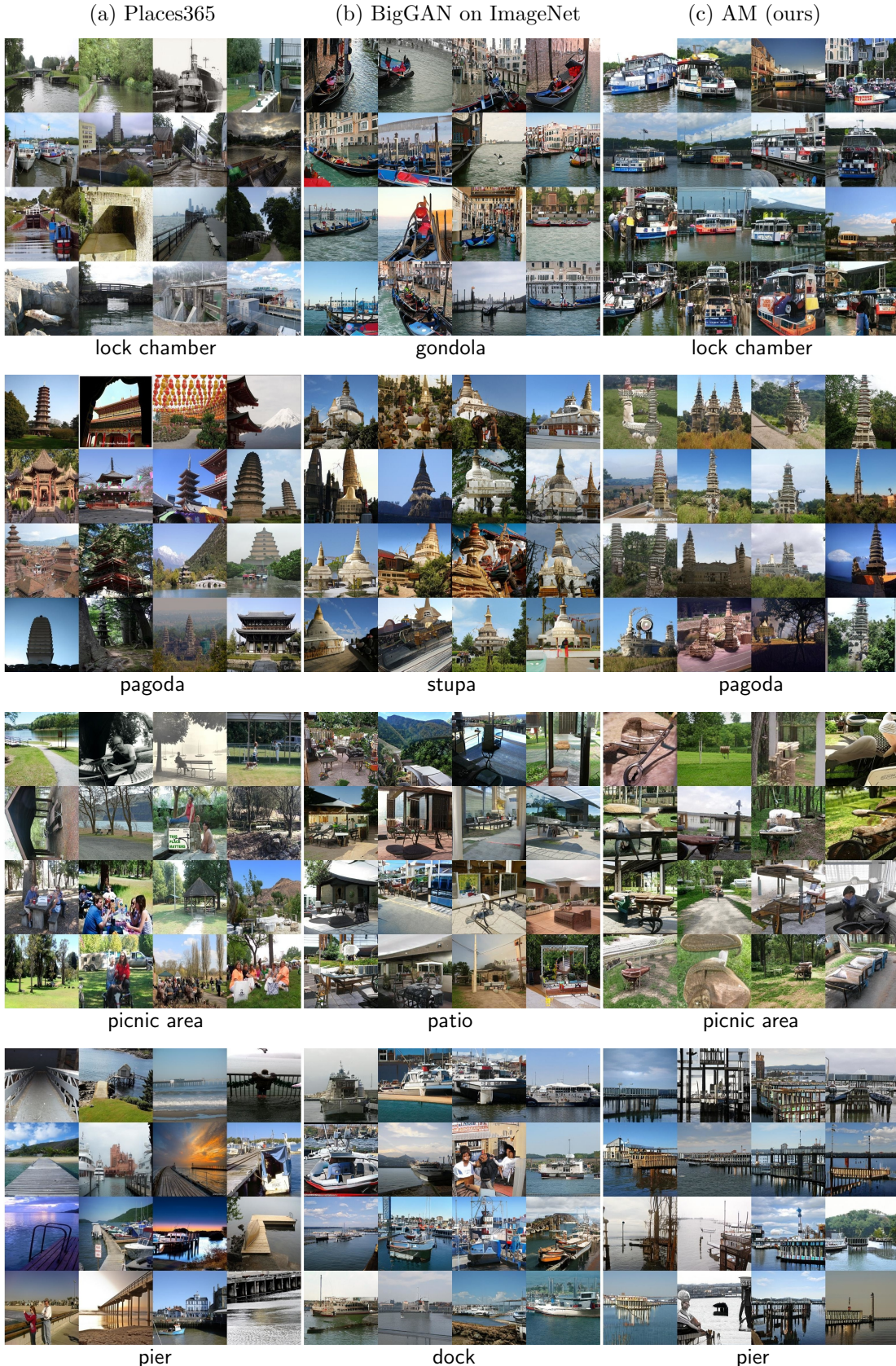


Figure S22: The same figure as Fig. S20 but for four different classes. In the bottom panel, while the BigGAN samples are dock images that contain mostly ships whereas AM samples show more bridges that resemble the real pier samples in Places365. See https://drive.google.com/drive/folders/1L-1ULPf0f_5-98I7emYW860PDu3Fjxn?usp=sharing for a high-resolution version of this figure.



Figure S23: The same figure as Fig. S20 but for four different classes. For the **baseball stadium**, the top-1 ImageNet class is **scoreboard** (b), an object commonly found in stadiums. However, the AM samples are more similar to the images from Places365, which often do not contain scoreboards (a vs. c). See https://drive.google.com/drive/folders/1L-1ULPf0f_5-98I7emYW860PDu3Fjxn?usp=sharing for a high-resolution version of this figure.